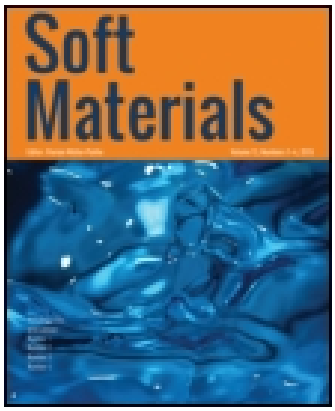

Soft Materials
Publication details, including instructions for authors and subscription information:
http://www.tandfonline.com/loi/lsfm20

Molecular Dynamic Study of the Structure and Dynamics of Polymer Melt at Solid Surfaces

Jalal Sarabadani[a], Andrey Milchev[ab], Andres De Virgiliis[c] & Thomas A. Vilgis[a]
[a] Max Planck Institute for Polymer Research, Mainz, Germany
[b] Institute of Physical Chemistry, Bulgarian Academy of Sciences, Sofia, Bulgaria
[c] INIFTA, La Plata, Argentina
Accepted author version posted online: 30 Aug 2014.Published online: 18 Nov 2014.

To cite this article: Jalal Sarabadani, Andrey Milchev, Andres De Virgiliis & Thomas A. Vilgis (2014) Molecular Dynamic Study of the Structure and Dynamics of Polymer Melt at Solid Surfaces, Soft Materials, 12:sup1, S56-S70, DOI: 10.1080/1539445X.2014.957833

To link to this article: http://dx.doi.org/10.1080/1539445X.2014.957833

Soft Materials (2014) **12**, S56–S70

ISSN: 1539-445X print / 1539-4468 online
DOI: 10.1080/1539445X.2014.957833

Taylor & Francis
Taylor & Francis Group

Molecular Dynamic Study of the Structure and Dynamics of Polymer Melt at Solid Surfaces

JALAL SARABADANI[1]*, ANDREY MILCHEV[1,2], ANDRES DE VIRGILIIS[3], and THOMAS A. VILGIS[1]

[1]*Max Planck Institute for Polymer Research, Mainz, Germany*
[2]*Institute of Physical Chemistry, Bulgarian Academy of Sciences, Sofia, Bulgaria*
[3]*INIFTA, La Plata, Argentina*

Received April 1, 2014; Accepted May 30, 2014

We investigate the dynamic and static properties of a polymer melt near solid surfaces. The melt, composed of linear chains, is confined between two solid walls with one of the walls being repulsive; whereas the opposite, attractive wall, is characterized by different degrees of roughness, caused by an array of short perpendicular pillars with variable grafting density. We demonstrate the remarkable fact that the conformations of chains in the melt at the interfaces are mostly unaffected by the strength of substrate/polymer attraction. Moreover, they practically coincide with the conformations of a *single* end-grafted chain at the *critical point of adsorption,* in agreement with Silberberg's hypothesis. This agreement is corroborated by the analysis of the size distributions of trains, loops, and tails of melt chains at the walls that are found to be perfectly described by analytical expressions pertaining to end-grafted *single* chains at critical adsorption. The adsorbed amount at the attractive bottom surface is found to scale with macromolecule length as $\Gamma \propto \sqrt{N}$ regardless of adsorption strength. We also find that the pressure of the melt P_{N} decreases as $P_N - P_\infty \propto N^{-1}$ (where P_∞ is the extrapolated pressure for $N \to \infty$) with growing length N of the chains whereas the surface tension γ at both walls is found to decline as $\gamma_N \propto N^{-2/3}$. Eventually, a study of the polymer dynamics at the rough interface reveals that surface roughness leads to dramatic drop of the coefficient for lateral diffusion whenever the separation between obstacles (neighboring pillars) becomes less than $\approx 2R_g$ where R_g is the unperturbed radius of gyration of chains in the bulk.

Keywords: Polymer melt, Dynamics, Pressure, Surface tension

Introduction

The structural and dynamic properties of polymer melts near solid substrates have been investigated for several decades (1). They are not only interesting from a fundamental point of view but also play a major role in various applications such as in lubricants, surface coatings, and composite materials, where these macromolecules can control the overall performance of the system (1, 2). Both the structural and dynamic properties of the macromolecules are modified by the presence of surfaces, in comparison with those in the bulk. To discover the range of surface effects on the melt and their origins, which are not well understood, Molecular Dynamics (MD) simulation studies can play a major role. For example, the effect of the strength of substrate-polymers adsorption or, instead, the result from the geometric constraints imposed by the confining wall is still a matter of repeated studies and debate (3). The presence of a wide range of length and time scales involved in the problems is the general reason they are not fully understood, which makes the experimental data analysis difficult (4).

In this sense, the use of computer-aided modeling for the study of confined polymer melts has proven to be rewarding. By means of computer simulations, a number of physically relevant quantities that describe the relaxation and structure of the polymer melt can be defined and also elucidated in detail. Two main approaches can be recognized in this field of research. In the case of *atomistic* simulations, the emphasis is mainly on the chemically realistic, detailed description of the systems and their properties. In this case some examples of recent works are the studies by Daoulas et al. (5, 6) on films of polyethylene on graphite; Mansfield and Theodorou (7–10) and Smith et al. (11) (atomistic surface/*n*-alkane); Pandey and Doxastakis (12) (silica/polyethylene); Yelash et al. (13) (graphite/polybutadiene); and Hentschke et al. (14) (graphite/alkane). A lot of information regarding polymer behavior at particular surfaces can be provided by means of these methods, as long as the concentrations are not too high. However, atomistic simulations are not feasible as a source of reliable statistical data, for concentrations approaching the melt conditions.

In order to be able to treat much larger systems with the proper statistical averaging of the observables, and also study systems for a longer period of time, one can alternatively use *coarse-grained* models whereby some atomistic details are sacrificed.

*Address correspondence to: Jalal Sarabadani, Department of Applied Physics and COMP Center of Excellence, Aalto University School of Science, P.O. Box 11000, FI-00076 Aalto, Espoo, Finland. Email: jalal.sarabadani@aalto.fi
Color versions of one or more of the figures in the article can be found online at www.tandfonline.com/lsfm.

Most frequently, by means of Monte Carlo (MC) methods (15–18) and MD (19–31) atomistic, as well as coarse-grained studies' are carried out. A rather efficient approach to analyze the structural properties is based on Self-Consistent Field (SCF) models at the level of mean-field approximation (32–34). Most of these computer experiments have been focused on the structure and relaxation dynamics of a polymer melt at solid (atomically smooth or structureless) substrates. It has been demonstrated, however, that a major influence may be due to differences in the smoothness of the solid boundary, for example, on fundamental aspects of the glass transition in polymer films [e.g., see (21–24, 35–39)]. A rather important aspect of this problem is the correlation amang structural, dynamical, and mechanical properties of polymer nanocomposites (40, 41).

In the present work, we consider the structure and dynamic properties of a linear polymer melt at solid interfaces, and we focus on several aspects that have' thus far, determined minimal or insufficient attention within the context of the properties of the interfacial melt. Following Silberberg's theoretical predictions (42, 43) and Skvortsov and Gorbunov (44), we demonstrate that in the confined melt, random walks with reflecting boundary (according to the so called Silberberg's hypothesis) can describe the conformations of a chain, and *irrespective* of the particular interaction between the solid substrate and the melt, these conformations are nearly identical to those of a *single* chain under *critical adsorption conditions* (45). In the previous works on this problem, where lattice models have been used (3, 17, 18) in contrast to continuum models, some typical properties of the melt structure near a solid wall such as the well-known packing or layering effect could not be reproduced. Therefore, the answer to the question as to what extent the Silberberg's hypothesis holds within the framework of a more realistic (off-lattice) description of the melt/substrate region has remained unclear. We examine the probability distributions of the trains, loops' and tails of polymers near the solid wall and find that they closely follow the theoretically predicted results by Fleer and colleagues (32, 33) and Hoeve et al. (46) for single polymer chains at the point of critical adsorption on a flat solid wall.

Moreover, in the present study, which is the mini review of our recent papers (27, 45), we examine carefully the behavior of pressure, P_{N}, exerted by the melt on the container surfaces, in particular, the impact of polymer length N on pressure. Our results show that $P_N(N) - P_\infty$ diminishes as N^{-1} with growing chain length while the surface tension, γ_N, which is derived from the pressure anisotropy parallel and perpendicular to the substrate, is found to change as $N^{-2/3}$, in agreement with some earlier experimental findings (see Pressure section). Eventually, we consider the dynamics of polymer melt in the presence of both smooth and rough surfaces. To study the impact of the different levels of the roughness on the dynamics, we consider a system where an array of vertical pillars with various grafting densities are grafted by the solid wall.

The remainder of the paper is organized as follows: In The Model section we introduce our coarse-grained model to study the solid/melt system and also the parameters of the MD simulation. The Static Properties of the Polymer Melt section is devoted to studies of statics properties of the chains in the confined melt, such as monomer number density; bond lengths and orientation; adsorbed amount; gyration radius, loops, trains, and tails distributions; and pressure across the container. In this section we present our test of Silberberg's hypothesis. In the Dynamics section, we show the results on the dynamics of the polymer melt at the vicinity of the confining walls. Our Summary is briefly described in the Conclusion section.

The Model

We use a coarse-grained bead-spring model of polymer chains (47) to study the properties of a polymer melt near hard walls. In this model, the bonded interaction between neighboring beads of a polymer is a combination of a finitely extensible nonlinear elastic (FENE) potential:

$$U_{\mathrm{FENE}} = -\frac{k_0}{2} R_0^2 \ln\left[1 - \left(\frac{r}{R_0}\right)^2\right], \tag{1}$$

where the elastic constant is $k_0 = 30$; and $R_0 = 1.5$ is the maximal extension of the bond between neighboring segments; and the Weeks-Chandler-Anderson (WCA) potential:

$$U_{\mathrm{WCA}}(r) = \begin{cases} U_{\mathrm{LJ}}(r) - U_{\mathrm{LJ}}(r_c), & r \le r_c, \\ 0, & r > r_c, \end{cases} \tag{2}$$

where the radius of cut-off is $r_c = 2^1/^6$; and $U_{\mathrm{LJ}}(r)$ is the Lennard-Jones (LJ) potential:

$$U_{\mathrm{LJ}}(r) = 4\epsilon\left[\left(\frac{\sigma}{r}\right)^{12} - \left(\frac{\sigma}{r}\right)^{6}\right], \tag{3}$$

where ϵ is the potential well depth, σ is the size of each monomer, and r is the distance between monomers. All quantities are defined in the reduced units, whereby the length is expressed in units of the LJ radius $\sigma = 1$, the mass of each monomer is set to $m = 1$, and the energy unit is $\epsilon = 1k_BT$ (k_B is the Boltzmann constant). The unit of temperature, T, is ϵ/k_B, and the time is measured in the units of $\sigma\sqrt{m/\epsilon}$.

Truncated and shifted LJ potential, Eq. (3), with $\epsilon = 1$ and the cut-off radius of $r_c = 2.5$, is used for all nonbonded monomer–monomer interactions. The polymer melt is confined between two surfaces that are flat and are modeled as two-dimensional square arrays of beads with lattice constant of $a = 1$. We have considered a polymer melt composed of monodisperse linear chains.

In this study, three different system sizes named A, B, and C were chosen. In system A the box dimensions are $L_x = 64$, $L_y = 32$, and $L_z = 40$, which is used in the Monomer Density Profiles section, the Radius of Gyration section, the Test of Silberberg's Hypothesis section, and the Pressure section. In system B the simulation box has edges of $L_x = L_y = 16$, and $L_z = 50$, used in the Effects of Surface Roughness on the Melt Mobility of Monomers in the section. System C has rectangular container as a simulation box with edge lengths $L_x = 20$, $L_y = 20$, and $L_z = 60$, which is considerably larger than the thickness of the adsorbed films. We use system C in the Properties of the Adsorbed Melt section. In system A, the chain lengths are varied between $10 \le N \le 240$, which spans from the disentangled to an entangled

regime, whereas in systems B the length of the chains is only 10, and in system C we use chains with lengths $N = 16$, 24, 32, 48, and 80.

In systems A and B, the bottom surface is attractive and its beads interact with the monomers via a full LJ potential, shown in Eq. (3). The depth of the potential well is chosen as $\epsilon_{\text{bot}} = 2.0$ and a cut-off radius as $r_{c,\text{bot}} = 2.5$. The interaction between the beads of the top repulsive wall and the monomers is WCA, with $r_{c,\text{top}} = 2^{1/6}$as cut-off radius, and $\epsilon_{\text{top}} = 1$. In system C, the interaction between bottom attractive surface with melt is LJ potential with $r_{c,\text{bot}} = 2.5$ and various values of potential well depth of $\epsilon_w = 0.5$, 1.0, 2.0, and 3.0 are used. It will be mentioned whenever we use systems A, B, and C.

In order to examine effects of surface roughness, we have studied surfaces with variable roughness, which is tuned by changing the density of fixed vertical pillars that are arranged in a regular squared array on the attractive surface (see Fig. 1). Each pillar is made of 20 fixed beads with radius 1σ and the distance between neighboring beads in each pillar is 0.5σ, making a pillar height of 10. Pillar particles interact with the monomers through a WCA potential in system of type A while they are attractive in systems of type B.

In system A, the attractive and repulsive surfaces are placed at $z = 0$ and $z = 40$, respectively, and the monomer density is taken as 0.88. In contrast, in system B, the attractive and repulsive surfaces are placed at $z = 0$ and $z = 50$, respectively; as a result, a free surface of the melt that refers to a liquid-vacuum interface is formed in the vicinity of the repulsive wall. In system C, the solid attractive surface is located at $z = 0$ and in order to prevent escaping of the chains from the simulation box in the z direction, a *soft wall* is placed at the upper side of the cell.

We have summarized information regarding the different types of systems in the Table 1.

To study systems A and B, the ESPResSo++ package was used to perform the simulations (48), whereas system C was simulated by the DL-POLY package (49). We integrated the equations of motion by using the velocity-Verlet algorithm. The time step was chosen as $dt = 0.005$, and using a Langevin thermostat with a friction coefficient $\gamma = 0.5$, the temperature was set to $T = 1$.

Static Properties of the Polymer Melt

This section is devoted to the static properties describing polymer chain conformations, such as monomer number density (MND); bond length, radius of gyration; and the distribution of building units such as trains, loops, and tails in the vicinity of solid walls. Also, the pressure exerted by the melt on the container walls and the resulting surface tension are considered. As the system is anisotropic in the z-direction, we studied the monomer number density and the gyration radius layer-wise.

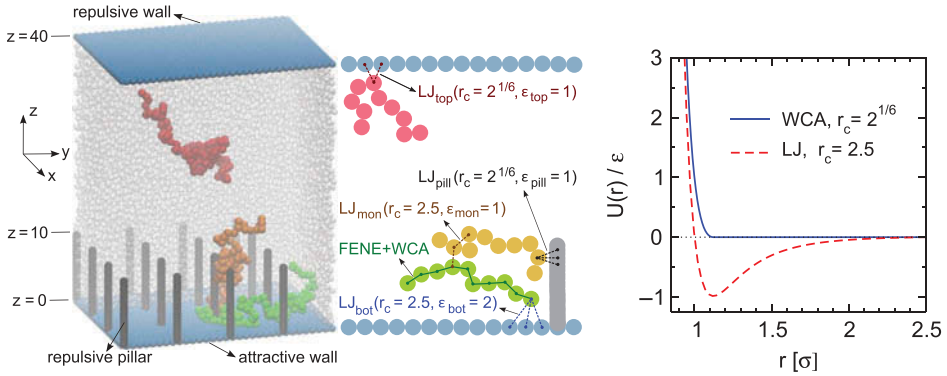

Fig. 1. Left panel: The schematic geometry of the system. The polymer melt is confined between a repulsive- (top), and an attractive wall (bottom). When surface roughness is considered, repulsive pillars with lengths of 10σ are attached vertically to the attractive wall. A polymer chain in the bulk (red) of the system and two chains (orange and green) near attractive wall are shown. The box size of the system is $L_x = 64$ (in the x direction), $L_y = 32$ (in y direction), and $L_z = 40$ (in z direction). For a better view we have cut the system and shown only part of it. Middle panel: different interactions that act in the system. Right panel: Normalized WCA and LJ potentials, $U(r)/\epsilon$, as a function of the distance between two particles, r. Reproduced from Sarabadani, J., et al. (45). ©2014, AIP Publishing LLC. Reproduced by permission of AIP Publishing LLC. Permission to reuse must be obtained from the rightsholder.

Table 1. Table of information for different systems A, B, and C.

System	$L_x \times L_y \times L_z$	N	ρ_r	Does it have free surface?	Sections
A	$64 \times 32 \times 40$	10–240	0.0–0.125	No.	Static properties
B	$16 \times 16 \times 50$	10	0.0–0.125	Yes.	Dynamics
C	$20 \times 20 \times 60$	16–80	0.0	Yes.	Static properties / Dynamics

First column: System type used in the simulations. Second column: Simulation box lengths in x (L_x), y (L_y), and z (L_z) directions, respectively. Third column: Lengths of polymer chains that have been used in each system. Fourth column: Pillar density. Fifth column: Availability of free surface. Sixth column: Indicates the sections where the particular systems is discussed.

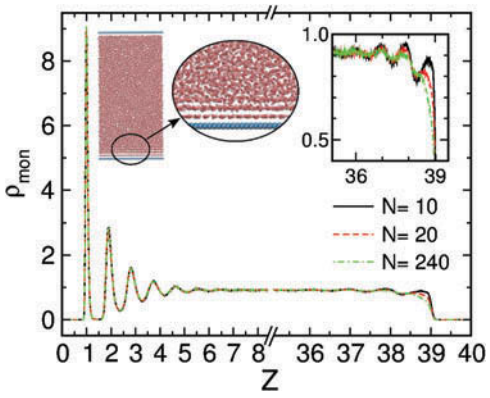

Fig. 2. The monomer number density profile, $\rho_{\text{mon}}(z)$, as a function of z, the distance from the bottom attractive surface, for different chain lengths of $N = 10$, 20, and 240. A snapshot of the system is presented in the left inset, where the layering effect can readily be seen. The region of $z > 37$ close to the upper repulsive container surface is magnified for better visibility. (Here, systems of type A have been studied.) Reproduced from Sarabadani, J., et al. (45). ©2014, AIP Publishing LLC. Reproduced by permission of AIP Publishing LLC. Permission to reuse must be obtained from the rightsholder.

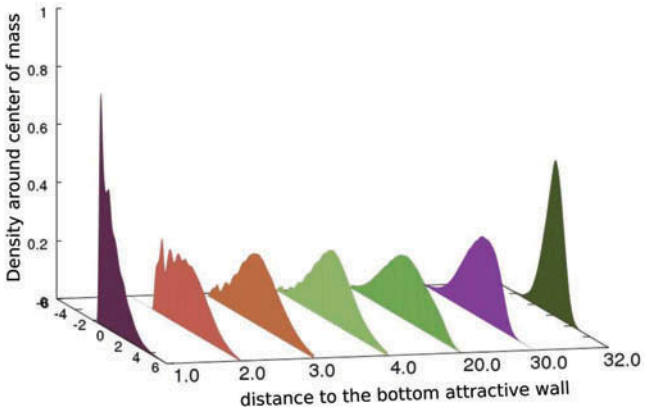

Fig. 3. Monomer distribution around the center of mass of the polymer chains, which are shown at different positions z across the film, as indicated. The adsorption strength of the attractive wall is $\epsilon_w = 2.0$ and the length of the polymer is $N = 80$. (Here, system of type C has been studied.) Reproduced from De Virgiliis, et al. (27). © Springer. Reproduced by permission of Springer. Permission to reuse must be obtained from the rightsholder.

Monomer Density Profiles

First, we consider the monomer density profile, $\rho_{\text{mon}}(z)$. Fig. 2 shows ρ_{mon} for three different systems composed of linear chains with lengths of $N = 10$, 20, and 240. To determine monomer number density, we divided each unit of length in the z direction into 100 slabs parallel to the container walls. As a rule, for systems composed of chain lengths $N < 240$, we averaged over 2×10^3 different realizations, and only for the systems with chain length of $N = 240$ the average was determined over 10^3 measurements. Apparently, a strong layering effect near the bottom attractive wall can be observed, whereas in the vicinity of the top repulsive wall this effect is weak. Near the bottom attractive surface all three density profiles coincide because, due to wall attraction, the melt monomers are rather densely packed at the bottom wall. In contrast, the layering effect in the vicinity of the top repulsive wall is only weakly pronounced. This small layering effect can be explained by looking at the behavior of the pressure as a function of chain length, which can be found in the Test of Silberbery's Hypothesis section (45). One can demonstrate the deformation of the chains close to the walls by analyzing the monomer distribution around the center of mass of each polymer chain for systems C. This quantity (see Fig. 3) is calculated across the melt and explains the mass rearrangements that polymer chains suffer due to the presence of the walls in more detail. The histograms reveal three main different regions. Chains close to the bottom attractive wall are strongly deformed and show a process of layering *inside* the polymer chain itself. This influence of the wall is screened and diminishes beyond a distance of approximately R_g, which is 4.9 for chain length of $N = 80$. At the middle of the film, around $z = 20.0$, the polymers display the expected, unperturbed Gaussian shape. Finally, close to the free surface, that is, around $z = 32.0$, the distribution of the density is getting slightly asymmetric with no layering.

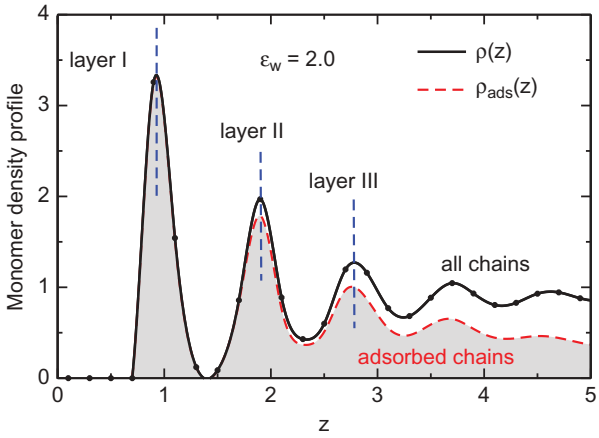

Fig. 4. Profile of the monomer density, $\rho(z)$, as function of the distance from the attractive wall z. Here, the chain size is $N = 80$ and the adsorption strength is $\epsilon_w = 2.0$. For better visibility, the monomer number density of those monomers that belong to the adsorbed chains only, $\rho_{\text{ads}}(z)$, is presented shaded in gray. Here, a typical layering effect for the first few layers parallel to the solid attractive surface can obviously be seen. (Here, system of type C has been studied.) Reproduced from De Virgiliis, et al. (27). © Springer. Reproduced by permission of Springer. Permission to reuse must be obtained from the rightsholder.

Properties of the Adsorbed Melt

In this subsection we focus on the properties of the *adsorbed* chains. To this end, first we look at the monomer number density profile once more. The overall variation of monomer density is presented in Fig. 4 as a function of the distance from the attractive wall, z, for a system of type C with chain length of $N = 80$ and $\epsilon_w = 2$. In this figure we differentiate between those monomers that belong to the adsorbed polymers (gray-shaded area) and the monomers belonging to chains with no contact with the wall. A typical layering effect for the mass distribution due to the

dispersive interactions is shown to decay beyond as approximate distance of $z = 5$. Therefore, the interphase region in the vicinity of the rigid attractive wall has a thickness of about 5 layers and this value does not vary with changing strength of the surface-chain attraction (see Figs. 2 and 4). One can use the first peak as a position of the so called *adsorption layer* whose thickness is about 0.9 of the diameter of a bead σ. In what follows, *adsorbed* chains are those polymers that have at least one monomer belongs to the first layer.

As the conformation of the chains in the vicinity of the substrate can determine many properties of the solid-polymer chain contacts, we focus on some features of the adsorbed layer. An important quantity to explore is the total mass of adsorbed chains, the so called *adsorbed amount* which is herein denoted by Γ. The adsorbed amount is defined as the total mass of those monomers that belong to the adsorbed polymer chains per unit of the surface area, and is equal to the area of the shaded region in Fig. 4. As mentioned earlier, an *adsorbed* chain refers to a polymer that contains at least one monomer in the region $0 < z < 1.4$ which is labeled by (I) in Fig. 4. The upper limit of this region, $z = 1.4$, is the position of the first minimum in the monomer number density profile $\rho(z)$ in Fig. 4. In Fig. 5 the adsorbed amount, Γ, is plotted as function of ϵ_w, which is the strength of the the attractive potential, for two different values of chain length $N = 32$ and 80. Before the adsorbed amount reaches a plateau, it increases steadily with growing strength of the attractive potential, ϵ_w. In the inset of Fig. 5, the saturating value of the plateau is plotted as a function of the chain length N and shown to behave as $\Gamma(N) \approx N^{1/2}$, which is fully in agreement with the theoretical prediction of Scheutjens and Fleer (50), and also with the atomistic simulation results of Daoulas et al. (5). For infinitely long single polymers, adsorption occurs when ϵ_w exceeds a certain *critical adsorption* value (51).

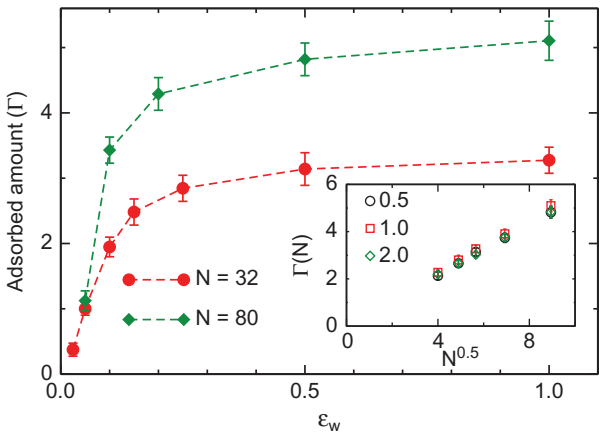

Fig. 5. The adsorbed amount Γ, which is defined as the total mass of monomers that belong to adsorbed polymer chains per unit area, is plotted as a function of the attractive potential strength, ϵ_w. The inset shows a good agreement with the theoretical prediction $\Gamma(N) \propto N^{1/2}$ (50), for various values of $\epsilon_w = 0.5$, 1.0, and 2.0. (Here, systems of type C have been studied.) Reproduced from De Virgiliis, et al. (27). © Springer. Reproduced by permission of Springer. Permission to reuse must be obtained from the rightsholder.

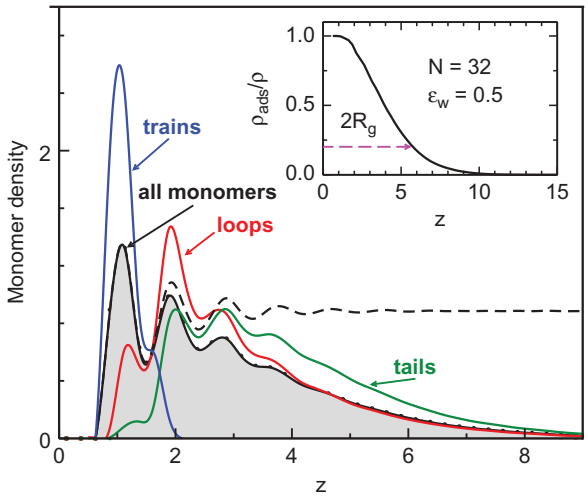

Fig. 6. Density profiles of adsorbed chains versus distance from the attractive substrate, z, for the case of weak adsorption strength of $\epsilon_w = 0.5$. The total number of adsorbed monomers, as highlighted by the gray shaded area, can be subdivided into three different building blocks of the chains: *loops*, *tails*, and *trains*. In the inset, the ratio $\rho_{ads}(z)/\rho(z)$, which can be used as a criterion to define the interphase region, is plotted as function of z. Analyzing the behavior of $\rho_{ads}(z)/\rho(z)$, one can determine the dependence of the thickness of the adsorbed layer, Δ_z, on the chain length as $\Delta_z \propto N^{1/2}$. (Here, system of type C has been studied.) Reproduced from De Virgiliis, et al. (27). © Springer. Reproduced by permission of Springer. Permission to reuse must be obtained from the rightsholder.

The polymers that contribute to Γ adopt different conformations that depend on the chain length and also on the surface-monomer interaction. Based on the definition of the adsorbed chains, one can distinguish between *trains*, which comprise successive monomers in a polymer chain all of which belong to the adsorbed layer, that is, are located within a distance closer than $z = 1.4$ to the substrate; *loops*, which are defined by successive monomers of a chain backbone that are themselves not adsorbed and connect two successive trains; and *tails*, which are the monomers of each end of the polymer that are located in the region $z > 1.4$. It can be seen in Fig. 6, that at short distances from the substrate, loops dominate over tails, whereas in the region outside of the adsorbed layer, both conformations of loops and tails are present. In contrast, within the adsorbed layer the trains dominate over tails and loops. In the inset, the ratio $\rho_{ads}(z)/\rho(z)$, which can be used as a criteria to define the interphase region, is plotted as a function of z. Looking at the behavior of $\rho_{ads}(z)/\rho(z)$, one can interpret the dependence of the thickness of the adsorbed layer, Δ_z, on the chain length as $\Delta_z \propto N^{1/2}$.

Distribution of Loops, Trains, and Tails

In this subsection we examine the distributions of tails, trains, and loops of the adsorbed polymers in the melt as main building units of the polymer architecture close to the confining walls. Based on the definition of the tails, loops, and trains in the previous part, we analyzed the trajectories resulting from the simulation of the systems of type A. We compare our simulation

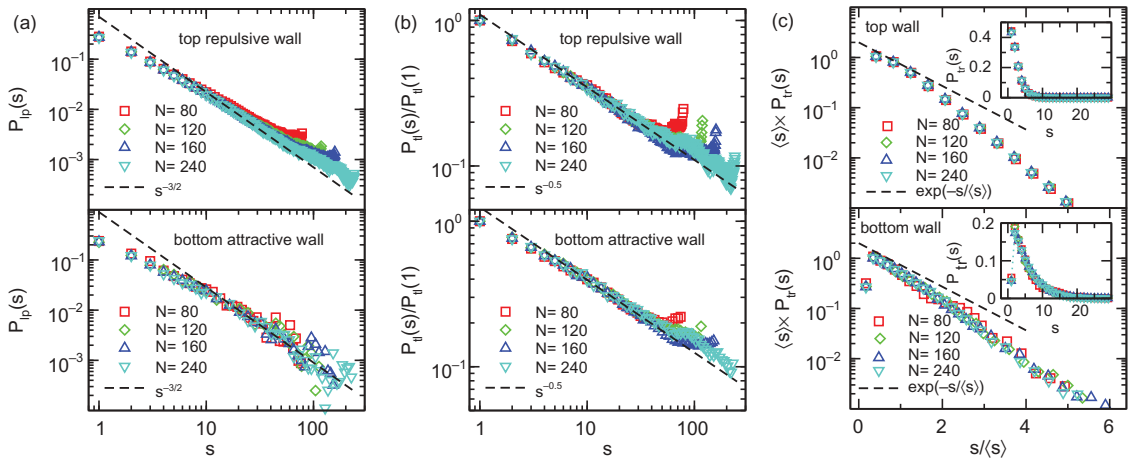

Fig. 7. (a) Distribution of loops near the top repulsive wall (top panel), and close to the bottom attractive wall (bottom panel), as a function of the length of the loop, s, for various values of polymer length, $N = 80$ (red squares), 120 (green diamonds), 160 (blue upward triangles), and 240 (turquoise downward triangles). The function $s^{-3/2}$ is denoted by the black dashed lines in both panels. (b) Normalized distribution of tails close to the repulsive (top panel) and near the attractive (bottom panel) surfaces as function of the tail length, s, for the same polymer length values as in (a). Here, the function $s^{-0.5}$ is indicated by the black dashed lines in both panels. (c) Normalized distribution of trains close to the repulsive (top panel) and near the attractive (bottom panel) surfaces as a function of the normalized length of trains, $s/\langle s\rangle$, where $\langle s\rangle$ is the train length mean value, for the same values of chain length, N, as of (a) and (b). The insets present the trains distribution as function of the train length, s, in *normal* coordinates. Black dashed lines denote $\exp(-s/\langle s\rangle)$. (Here, systems of type A have been studied.) Reproduced from Sarabadani, J., et al. (45). ©2014, AIP Publishing LLC. Reproduced by permission of AIP Publishing LLC. Permission to reuse must be obtained from the rightsholder.

results also with theoretical predictions, since there are several detailed predictions about the size distribution of tails, loops and trains for a *single* polymer under conditions of critical adsorption (32, 46, 52, 53).

In Fig. 7(a) the distributions of the loops close to the repulsive (top panel) and near the attractive (bottom panel) surfaces are plotted as a function of the length of the loop, s, for various values of the polymer length, $N = 80$, 120, 160, and 240. The predicted power law function $s^{-3/2}$ is denoted by the black dashed lines. Apparently, apart from some deviations for the shortest loops, $s \leq 4$, and the poor statistics in the measurements of the longest loops, one can observe a rather good agreement in the intermediate region of s where the available statistics is reliable. In Fig. 7(b), the normalized distribution of polymer tails near the top repulsive (top panel) and the bottom attractive (bottom panel) surfaces have been presented as function of the length of the tail, s, for the same polymer lengths as in (a). Again one, can see that the power law dependence $s^{-0.5}$ perfectly describes the distribution of tails (which covers a broad range of tail sizes). In Fig. 7(c), one can find some deviations (an initial power law relationship at small values of *s)* from $\exp(-s/\langle s\rangle)$ (where $\langle s\rangle$ is the mean value of the length of trains) which is the theoretical prediction. The absolute value of the negative slope of the exponential distribution function is also some what smaller than the inverse of the mean value of *s,* that is, $1/\langle s\rangle$. We believe that this occurs because of the uncertainty (arbitrariness) in the definition of the trains itself, which makes the distinction between flat loops and short trains a matter of convention in continuous models. As it can be seen from the insets, on the average, one can find longer trains close to the attractive surface in comparison with the repulsive wall.

In summary, after analysis of the size distributions of all three building units of polymer chains that are in contact with the solid surfaces, one can suggest again that the conformations of the adsorbed chains in a melt, *irrespective of the wall-chain interactions,* are exactly the same as those of a single chain in a dilute solution at the critical adsorption point (CAP). It should be mentioned that these results support the similar findings on the probability distributions of tails, loops, and trains, which were recently derived on a lattice (3).

Radius of Gyration

Another basic quantity is the gyration radius, R_g, which is defined as:

$$R_g^2 = \frac{1}{N}\sum_{i=1}^{N}(\vec{R}_i - \vec{R}_{\rm cm})^2 \qquad (4)$$

where the radius-vector of the center of mass of each chain is $\vec{R}_{\rm cm}$ (54), and the end-to-end distance is R_e. The latter is obtained by considering only those chains that have their centers of mass inside a slab in the middle of the system with a thickness equal to the gyration radius.

The effect of confining surfaces on the chain conformations can be examined by studying the variation of the perpendicular, $R_{g\perp}^2 = \frac{1}{N}\sum_{i=1}^{N}(z_i - z_{\rm cm})^2$ and the parallel, $R_{g||}^2 = \frac{1}{2N}\sum_{i=1}^{N}\left[(x_i - x_{\rm cm})^2 + (y_i - y_{\rm cm})^2\right]$, components of R_g^2. In Fig. 8 the scaling behavior of R_g^2, $R_{g\perp}^2$, and $R_{g||}^2$ is shown for different regions: the bulk, the first ($z < R_g$), and the last ($L_z - z < R_g$) layers as function of the polymer length, N. The thickness of the

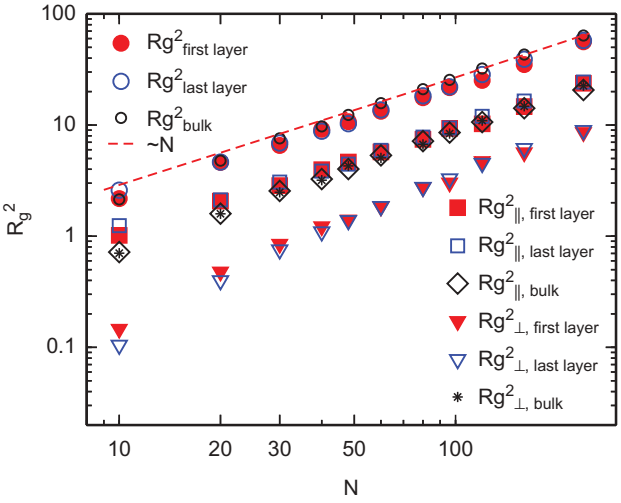

Fig. 8. R_g^2 for the first layer (filled red circles), for the last layer (open blue circles), and for the bulk (open black circles); $R_{g||}^2$ for the first layer (filled red squares), for the last layer (open blue squares) and for the bulk (open black diamonds); and $R_{g\perp}^2$ for the first layer (filled red triangles), for last layer (open blue triangles), and for the bulk (black stars), plotted as a function of polymer length, *N*. The first layer is located at the bottom attractive wall while the last layer is at the top repulsive wall. The thickness of both of them is the same and equal to the radius of gyration in the bulk of the system. (Here, systems of type A have been studied.) Reproduced from Sarabadani, J., et al. (45). ©2014, AIP Publishing LLC. Reproduced by permission of AIP Publishing LLC. Permission to reuse must be obtained from the rightsholder.

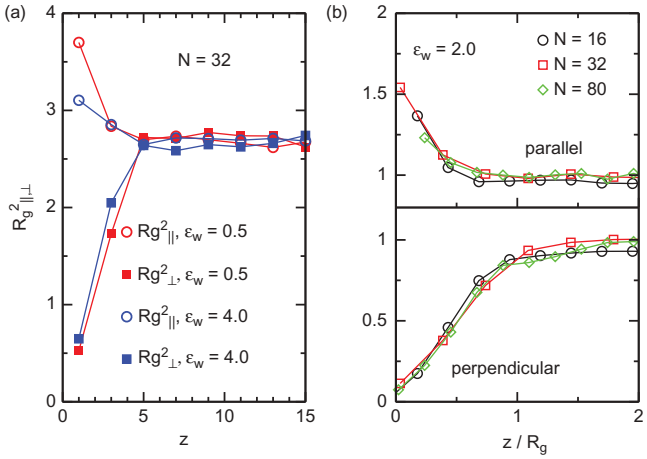

Fig. 9. (a) Profiles of the squared parallel (circles) and perpendicular (squares) components of the gyration radius as function of the distance from the attractive wall for two values of the adsorption strength, $\epsilon_w = 0.5$ and 4.0. (b) Top panel: Squared parallel component of the gyration radius as function of the normalized distance to the attractive wall, z/R_g, for three different values of the chain lengths $N = 16$, 32, and 80 at fixed value of the adsorption strength $\epsilon_w = 2.0$. Bottom panel: The same as the top panel but for the perpendicular component. Here, we study systems of type C in both (a) and (b). Reproduced from De Virgiliis, et al. (27). © Springer. Reproduced by permission of Springer. Permission to reuse must be obtained from the rightsholder.

first and the last layers is equal to the bulk value of $\sqrt{\langle R_g^2 \rangle}$ for each N. Interestingly, the parallel and perpendicular components of the radius of gyration in the first (solid red square and downward triangles, respectively) and also in the last layers (open blue square and downward triangles, respectively) vary in such a way that the *total* gyration radii in these layers (solid red and open blue circles, respectively) remain almost equal to that of the bulk region of the system (open black circles) for each polymer length. Therefore, the particular (attractive/repulsive) interactions of the surface with the melt may make a minimal difference in the conformational properties of the adjacent chains.

In Fig. 9(a) the squared parallel (circles) and perpendicular (squares) components of the gyration radius are plotted as a function of the distance from attractive wall, *z,* for two values of the adsorption strength, $\epsilon_w = 0.5$ and 4.0. The top panel of Fig. 9(b) shows the squared parallel component of the gyration radius as function of the normalized distance to the attractive wall, z/R_g, for three different values of the chain lengths $N = 16$, 32, and 80 at fixed value of the adsorption strength $\epsilon_w = 2.0$. Similarly, in the bottom panel the perpendicular component of the radius of gyration is presented. In Fig. 9(a) and (b) we study systems of type C. These results are fully in agreement with earlier studies of computer simulations (55, 56) as well as with theoretical works (57, 58). Apparently, the polymer coil deformation vanishes at distances $z \geq Rg$. Apparently, only a small increment in the chain deformation is due to the increase in the adsorption potential strength, ϵ_w.

Test of Silberberg's Hypothesis

In this section we present our MD simulation data to test the theory of Silberberg (42, 43), which explains the average contraction of macromolecules in the vicinity of a solid-melt interface in terms of a set of principles for "conformation transfer," which involves "segmental swapping" between unconstrained chains with regard to the confining hard wall. The polymers are labeled by their "starting monomer" (that polymer end which is closer to the solid wall). Using Silberberg's procedure of reflection of configurations, one can reproduce the dominant features of a melt at a solid wall interface, and the most striking one is that the polymer chain conformations are, thereby, entirely insensitive to the existing (attractive or repulsive) polymer- wall interaction!

This intuitively unexpected theoretical prediction has not generated only minimal attention by researchers (3, 17). Bitsanis and ten Brinke (17) mentioned that the chains can be modeled as Gaussian coils, provided the "reflective" boundary condition, introduced by Silberberg (42, 43), is applied to *statistical*, rather than to the actual segments, although the statistical segment inside the bulk may not be identical with those at the interface. Therefore, in this subsection we tested the extent of the presence of an interface (as, e.g., the observed layering effect immediately at the container surfaces) can influence Silberberg's predictions.

To check the validity of Silberberg's theory for the random walk statistics close to a reflective boundary in reproducing actual chain conformations at solid-melt interfaces, we present in Fig. 10 simulation data for the "chain start" probability $P_{\text{start}}(z)$ and compare them with the corresponding analytical result (42,

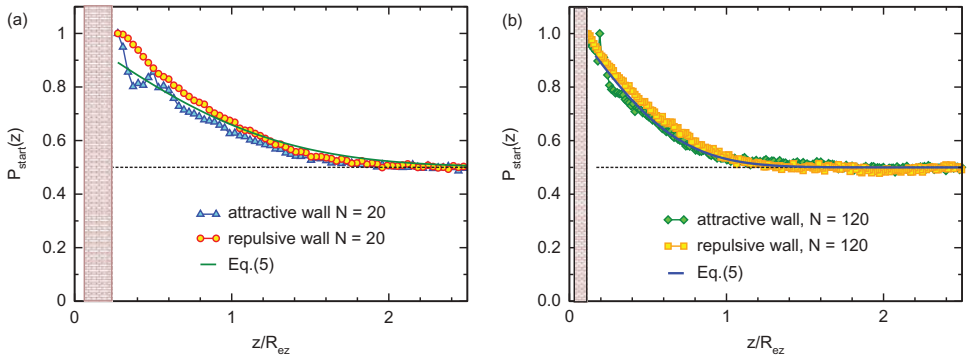

Fig. 10. (a) Density profiles of chain "starts", $P_{start}(z)$, i.e., the probability that an end of a chain is found at a particular distance z from the wall, for chain size $N = 20$. Both a repulsive surface (red circles) and an attractive surface (blue triangles) are examined. A chain start is defined as the chain end that is closer to the wall. The analytical prediction is indicated by the green line. (b) The same as (a), but for chain length $N = 120$. (Here, systems of type A have been studied.) Reproduced from Sarabadani, J., et al. (45). ©2014, AIP Publishing LLC. Reproduced by permission of AIP Publishing LLC. Permission to reuse must be obtained from the rightsholder.

43). A chain start is defined as the chain end closest to the surface. $P_{start}(z)$ is the probability of finding a chain end monomer at distance z from the surface, provided this monomer is a chain start. As it can be seen, P_{start} equals $1/2$ in the bulk (i.e., each chain end may be the closer one with 50% probability) and approaches unity immediately at the surface where the chance to find the second chain end at the same distance nearly vanishes. The analytical relation for $P_{start}(z)$ is

$$P_{start}(z) = 1 - \frac{1}{2}\mathrm{Erf}\left(\frac{z}{\sqrt{2}R_z}\right) \tag{5}$$

where Erf(z) is the error-function (42, 43).

It can be seen that the simulation data is confirmed reasonably well by the prediction in Eq. (5), for *both* surfaces apart from some oscillations near the attractive wall, due to the layering effect. Note, that layering at the walls is due to the excluded volume interactions between the monomers and reflects packing effects of the monomers (which are themselves treated as soft spheres within the MD simulation). Silberberg's theory completely ignores the excluded-volume interactions and considers the polymer chains in the melt as random walks, that is, as ideal Gaussian chains, as the Flory exponent of a polymer chain in a melt is $\nu = 1/2$, as this is the case for ideal chains. Therefore, our MD data reveal additional details that are beyond the scope of Silberberg's theory. On the other hand, apart from the oscillations due to layering, the analytic expression, Eq. (5), agrees with our data remarkably well. Indeed, in Fig. 10 one can see that, regardless of the length of the chain, and irrespective of whether the solid wall repels or attracts the polymers, all data nearly collapse on a single master curve.

Eventually, we investigate the profiles of the concentration perpendicular to the surfaces for polymers whose starting ends reside immediately or very near to one of the surfaces such that these polymers may be considered as incidentally "grafted" to the solid wall. For a grafted chain, an analytical solution (52) for the overall distribution of polymer segments can be provided by using a continuum model for a *single* end-attached polymer under conditions of *critical adsorption*, $\phi_0(z)$, as well as for the distribution of polymer ends, $\phi_e(z)$:

$$\phi_e(z) = \frac{2}{\sqrt{\pi}R_g}\exp\left[-z^2/(4R_g^2)\right], \tag{6a}$$

$$\phi_0(z) = \frac{2}{\sqrt{\pi}R_g}\left\{\exp\left[-z^2/(4R_g^2)\right] - \frac{\sqrt{\pi}z}{2R_g}\,\mathrm{Erfc}\left(\frac{z}{2R_g}\right)\right\} \tag{6b}$$

where Erfc(x) is the complementary error-function. At the critical adsorption point (CAP), as is well known (3), the weak attraction, which is exerted by a flat surface on a polymer, compensates the entropy loss of the chain in the region near the surface, that is, segment enrichment goes over to depletion in such a way that the probability to find a polymer chain segment at some distance z from the surface does not depend on z. This effect holds irrespective of the concentration of chain in the container (3)! It can be argued that at the CAP the wall is, therefore, invisible for the chain due to a mutual compensation of enthalpic gain (i.e., attraction to the wall by the surface potential) and entropic loss owing to confinement.

From Figs. 11 and 12 one may readily verify that all the polymers of the melt that incidentally happen to touch with an end-monomer on either the repulsive or the attractive container walls, show distributions of the end- and all-segment density along z that are in good agreement with the analytical result, Eq. (6), of a single polymer chain at criticality. Skvortsov et al. (3), who applied the SCFT approach (i.e., worked within a Mean-Field Approximation approach) to a polymer melt on a cubic lattice, confirmed the same important conclusion that can be interpreted from Figs. 11 and 12.

Indeed, at high concentration (in the melt) polymer conformations in the vicinity of the constraining surfaces transform into the same type of half-Gaussian conformations of a random walk reflected by these surfaces, regardless of whether the melt adheres or not to the surface plane (3, 42, 43). The novel feature, detected in our MD investigation, are the oscillations, due to the layering effect near the surfaces, Figs. 11(a), and 12(a). Of course, these oscillations are not taken into account by the analytic theory (42, 43) and certainly cannot be reproduced by lattice model simulations. From Figs. 11(a) and 12(a), one may

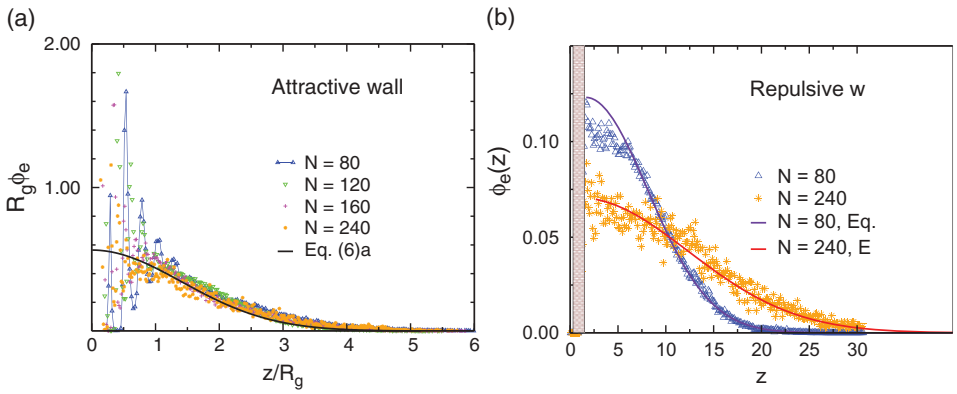

Fig. 11. Profiles of the density distribution of end-monomer $\phi_e(z)$ (symbols) versus distance from the solid attractive (a) and repulsive (b) surfaces z in a melt with chain sizes of $N = 80$ and 240. Only those chains are selected and analyzed whose ends incidentally touch the surfaces so that such chains may be considered as temporally "grafted." Solid lines indicate the analytic result for ideal Gaussian chains, Eq. (6a). (Here, systems of type A have been studied.)

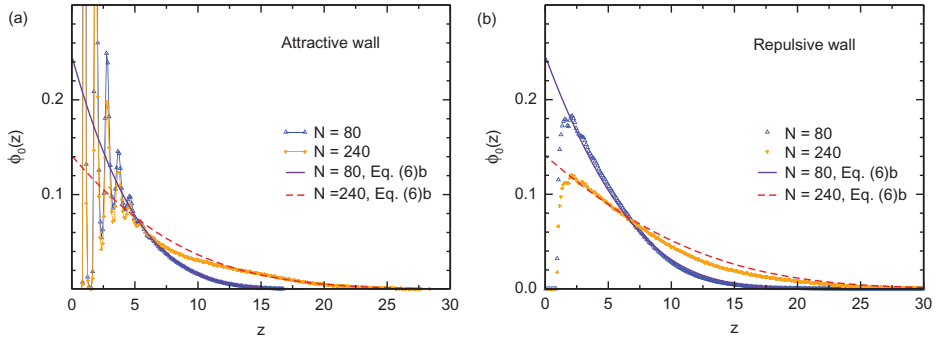

Fig. 12. Plot for the profiles of the monomer density, $\rho_{\text{mon}}(z)$, (symbols) against the distance z from an attractive (a), and repulsive surfaces (b), for chain lengths $N = 80$ and 240 in a melt. Lines indicate $\phi_0(z)$, which is the analytic expression for a Gaussian chain, Eq. (6b). (Here, systems of type A have been studied.)

easily discover that these oscillations occur only within the range of $z \leq 5$ and do not depend on the macromolecules length N. Apart from these oscillations, however, one may argue that one can describe the chain conformations in the melt as random walks that are reflected at the solid surface.

Pressure

We studied the pressure profile across the slit as a function of the z-coordinate for different values of the polymer length N. The pressure tensor is written as a sum of the virial, P_{U}, and kinetic, P_{K} parts (20). The statistically averaged values of all off-diagonal elements of the pressure tensor equal zero, as the system under consideration is in mechanical equilibrium state. Moreover, due to the geometrical symmetry of the system, the lateral components of the pressure tensor, that is P_{xx} and P_{yy}, are equivalent to one another.

The pressure tensor is written as $P(z) = \mathbf{e}_z\mathbf{e}_z P_{\text{N}}(z) + (\mathbf{e}_x\mathbf{e}_x + \mathbf{e}_y\mathbf{e}_y)\, P_{\text{T}}(z)$, where $\mathbf{e}_x$, $\mathbf{e}_y$, and $\mathbf{e}_z$ are unit vectors in x, y, and z directions, respectively. By means of Irving and Kirkwood's (IK) method, we computed both the normal, P_N (z), and lateral, P_{T} (z), components of the pressure tensor layer-wise (59). Using Irving and Kirkwood (59), we take only the contribution of pairwise forces between particles to the virial part into account, provided the connecting line of the centers of mass of these particles intersects the infinitesimal surface of $d\vec{A}(z)$. The tensor for the pressure, P, is itself defined as $d\vec{F} = -d\vec{A}P$ where $d\vec{F}$ is an infinitesimal force. Using the IK method and the definition for the virial contribution to pressure, that is, P_{U} (60), one can write the averaged value of the normal and tangential components of the pressure tensor layerwise as:

$$P_{\text{N}} = \rho(z)k_BT - \frac{1}{2A}\left\langle \sum_{i\neq j=1}^{N_{tot}} \frac{|z_{ij}|}{r_{ij}} U'(r_{ij})\,\Theta\left(\frac{z-z_i}{z_{ij}}\right)\Theta\left(\frac{z_j-z}{z_{ij}}\right)\right\rangle, \tag{7a}$$

$$P_{\text{T}} = \rho(z)k_BT - \frac{1}{4A} \left\langle \sum_{i\neq j=1}^{N_{tot}} \frac{x_{ij}^2+y_{ij}^2}{r_{ij}} \frac{U'(r_{ij})}{|z_{ij}|}\Theta\left(\frac{z-z_i}{z_{ij}}\right)\Theta\left(\frac{z_j-z}{z_{ij}}\right)\right\rangle, \tag{7b}$$

where A is the surface area of the system that is parallel to the $x-y$ plane; $\rho(z)$ is the value of the number density of the monomers, averaged over lateral coordinates x and y; and the summation runs over all pairs of particles with N_{tot} being the the total number of

monomers in the system. Note that N_{tot} includes the (static) particles comprising the walls of the slit too. Here, $\langle\bullet\rangle$ denotes the statistically averaged value of the quantity $\bullet$. In Eq. (7a, b), r_{ij} is the distance between the particle i and the particle j, with the definition of $\mathbf{r}_{ij} = \mathbf{r}_i - \mathbf{r}_j$, $\mathbf{r}_{ij} = |\mathbf{r}_{ij}|$, and the three different components of $\mathbf{r}_{ij}$ are x_{ij}, y_{ij}, and z_{ij}. The derivative $-U'(r_{ij})$ of the potential U is the force between particles i and j, and the Heaviside step function is denoted by $\Theta(x)$. In Eq. (7a, b), the first term is the kinetic part of the pressure. To calculate the normal and tangential components of the pressure tensor, we combine Eq. (7a, b) with the following identity:

$$|z_{ij}|\Theta\left(\frac{z-z_i}{z_{ij}}\right)\Theta\left(\frac{z_j-z}{z_{ij}}\right) = -z_{ij}[\Theta(z_i-z)\Theta(z-z_j)-\Theta(z_j-z)\Theta(z-z_i)]. \quad (8)$$

In Fig. 13, the variation of the normal component of the pressure tensor, $P_N - P_\infty$, is plotted as a function of chain length for several pillars grafting densities, ρ_r, N, where P_∞ is the value of P_N extrapolated to the limit of $N \to \infty$ for each value of the grafting density of pillars, ρ_r.

As the Irving-Kirkwood method is valid only for systems with lateral translational symmetry (59), the pressure is measured across the whole systems when $\rho_r = 0$, whereas for systems with $\rho_r \neq 0$, the pressure is calculated only for the region of $z > 20$. As expected, the inset in Fig. 13, shows a systematic increase in P_N with the growing in the density of pillars, which is due to the decrease in the total accessible volume in the container, cf. Fig. 13(b).

Interestingly, irrespective of the grafting density of pillars, the value of the difference $P_N - P_\infty$ collapses onto a single master curve, with the behavior of $P_N - P_\infty \propto 1/N$. In systems with pair interactions, the theoretical predictions confirm the aforementioned result (61). Indeed, the kinetic contribution to the normal pressure will remain when P_∞ is subtracted from P_N, which is proportional to the number of objects (in our case chains) in the system. A result of the decrease in the pressure with growing polymer length is to create a weaker layering effect near the top repulsive wall, which is presented in the right inset in Fig. 2, as the monomers are less tightly packed.

Another important and interesting quantity, studied also in this part, is the surface tension of the polymer melt at the top (repulsive) and the bottom (attractive) surfaces (for a system without pillars). By integrating the asymmetry of the pressure tensor, $P_N - P_T$, over z, the surface tension, can be obtained (20, 62, 63):

$$\gamma_{bot} = \int_{z=0}^{z=D_1} [P_N(z) - P_T(z)]dz, \qquad \gamma_{top} = \int_{z=D_2}^{z=40} [P_N(z) - P_T(z)]\,dz, \quad (9)$$

where D_1 and D_2 correspond to appropriate distances away from the two surfaces where the tangential and the normal components of the pressure tensor are statistically the same, that is., $P_N\ (z = D_i) - P_T(z = D_i) = 0$, and $i = 1, 2$. The surface tension γ at both interfaces of the system is plotted in Fig. 14. One can observe a power-law relationship, $\gamma(N) - \gamma_\infty \propto N^{-n}$ with the exponent of $n \approx 0.66 \pm 0.04$ by subtracting the extrapolated value of γ_∞ for infinitely long chains, that is, $N \to \infty$, in agreement with the predictions of the Cahn-Hilliard theory (64, 65) and with the experimental measurements of linear perfluorinated alkane melts (66–68).

Higher molecular weight of the polymers, a stronger dependence, $\gamma \propto N^{-1}$, has also been observed in experiments (67). However, these results have been challenged (68). The data for our longest polymers, $N = 240$, are derived within considerable error bars from our MD study; therefore, our result does not constitute an unambiguous check of n in this respect. In fact,

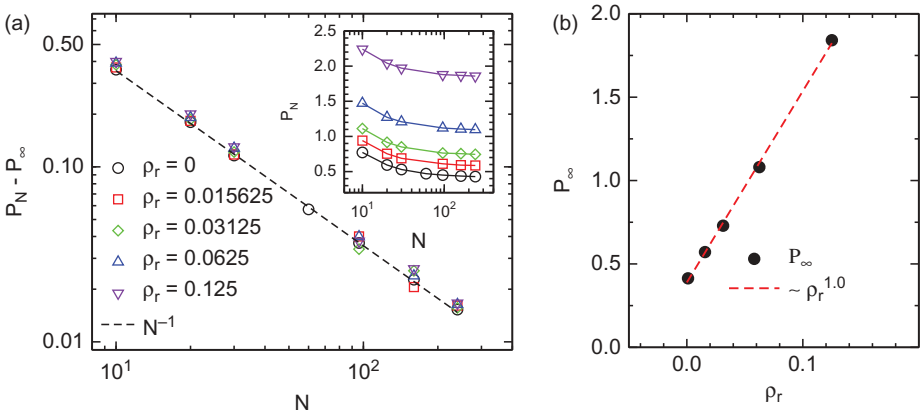

Fig. 13. (a) Inset shows P_N as function of the polymer length, N, for smooth walls (no surface roughness), and also for various values of the pillars density, $\rho_r = 0$ (black circle line), 0.015625 (red square line), 0.03125 (green diamond line), 0.0625 (blue upward triangles line), and 0.125 (violet downward triangles line). The main panel presents $P_N - P_\infty$ as a function of the polymer length, N, with the same values for the pillars density which are shown in the inset. (b) Here, the change in P_∞ (filled black circles) as a function of pillars grafting density, ρ_r, is shown. The red line is a fitting curve to the data points with an exponent of 1. (Here, systems of type A have been studied.) Reproduced from Sarabadani, J., et al. (45). ©2014, AIP Publishing LLC. Reproduced by permission of AIP Publishing LLC. Permission to reuse must be obtained from the rightsholder.

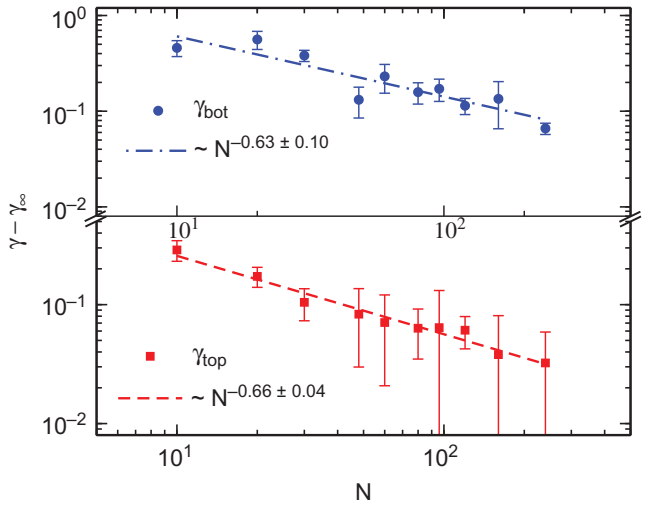

Fig. 14. Plot of the surface tension of the melt at the top repulsive surface, γ_{top}, and at the bottom attractive surface, γ_{bot}, as a function of the polymer length, *N*. In both cases we have subtracted the value γ_∞ extrapolated for $N \to \infty$. In both cases, the measured exponent n of $\gamma - \gamma_\infty \propto N^{-n}$ is in a good agreement with the experimentally measured value of $n = 2/3$ (66–68). (Here, systems of type A have been studied.) Reproduced from Sarabadani, J., et al. (45). ©2014, AIP Publishing LLC. Reproduced by permission of AIP Publishing LLC. Permission to reuse must be obtained from the rightsholder.

the experimentally observed variations of γ with the molecular weight can be reproduced by using the Cahn-Hilliard theory (67), such that both the $N^{-2/3}$ to N^{-1} dependence of γ can be derived and must be due to a variation in the properties of the bulk such as compressibility and density with changing *N*.

Dynamics

In this section we study the dynamics of melt at the flat and rough attractive walls. To this end, in the following Dynamic Properties Flat Wall Section, the influence of the flat attractive wall with different values of the attraction potential strength on the dynamics of the melt will be considered; whereas, in the Effects of Surface Roughness on the Mobility of Monomers in the Melt Section, the effect of surface roughness was investigated.

Dynamic Properties, Flat Walls

In this section, we present our findings on the dynamical properties of the melt at the interface. The dynamics of the system becomes anisotropic due to the presence of the walls. Therefore, one must distinguish between perpendicular and parallel directions. It is interesting to consider the effect of both free surface and the solid-polymer interface on the polymer chain dynamics (here, systems of type C are studied). According to previous studies (21, 35) and, in order to formulate the impact of these interfaces on the dynamics of the system, a *z*–dependent mean square displacement (MSD) for monomers is defined as:

$$g_0^{\parallel}(z,t) = \left\langle \frac{1}{n_t} \sum_i \prod_{t'=0}^{t} \delta(z - z_i(t')) \left| r_i^{\parallel}(t) - r_i^{\parallel}(0) \right|^2 \right\rangle,$$
$$g_0^{\perp}(z,t) = \left\langle \frac{1}{n_t} \sum_i \prod_{t'=0}^{t} \delta(z - z_i(t')) \left| r_i^{\perp}(t) - r_i^{\perp}(0) \right|^2 \right\rangle \quad (10)$$

In the aforementioned definition only those monomers, n_t, which remain at *all* times $t' \leq t$ within a given slab, are taken into account. We assume that z is the location of the center of each slab from the substrate.

To quantify to what extent the dynamics is influenced by the surface, a relaxation time τ_0, can be defined by the condition:

$$g_0^{\parallel}(z, t \equiv r_0^{\parallel}) = 1 \quad (11)$$

Characteristic times $\tau_0^{\parallel}$ and $\tau_0^{\perp}$ for displacements parallel and perpendicular to the substrate can be extracted by looking at $g_0^{\parallel}(z, t \equiv r_0^{\parallel})$ and $g_0^{\perp}(z, t \equiv r_0^{\perp})$, respectively. In Fig. 15, these quantities are plotted for two values of the adsorption potential strength $\epsilon_w = 0.5$ and 2.0 and for chain length of $N = 16$. Apparently, near the attractive wall, the behavior of the dynamics is qualitatively different, depending on ϵ_w. Fig. 15(a) shows that in the case of weak adsorption, the dynamics parallel to the wall is getting *faster* when approaching the wall, which means that the monomers almost slide at the wall. This effect is due to the fact that the layering effect is less pronounced in this case. Similar behavior is observed in other simulation studies [cf. Peter et al. (21)]. In contrast, one can see in Fig. 15(b) that in the regime of strong adsorption, when approaching the substrate, both characteristic times, $\tau_0^{\parallel}$ and $\tau_0^{\perp}$, rapidly grow. On the other hand, at the free surface one can see that the dynamics is faster as compared to the center of the melt, due to the local decrease in monomer density. As a rule, $\tau^{\perp} > \tau^{\parallel}$. Even in the center of the melt $\tau^{\perp}$ and $\tau^{\parallel}$ do not coincide, in agreement with earlier findings (35),

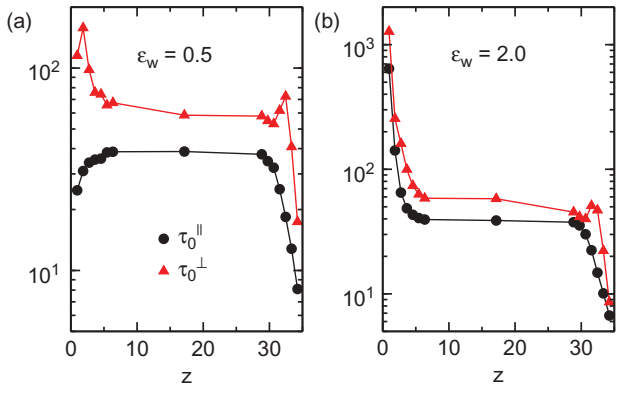

Fig. 15. Parallel and perpendicular relaxation times, $\tau_0^{\parallel}$ and $\tau_0^{\perp}$, respectively, for a system composed of linear chains with length of $N = 16$, for two values of the attraction potential strength $\epsilon_w = 0.5$ (a), and $\epsilon_w = 2.0$ (b). (Here, systems of type C have been studied.) Reproduced from De Virgiliis, et al. (27). © Springer. Reproduced by permission of Springer. Permission to reuse must be obtained from the rightsholder.

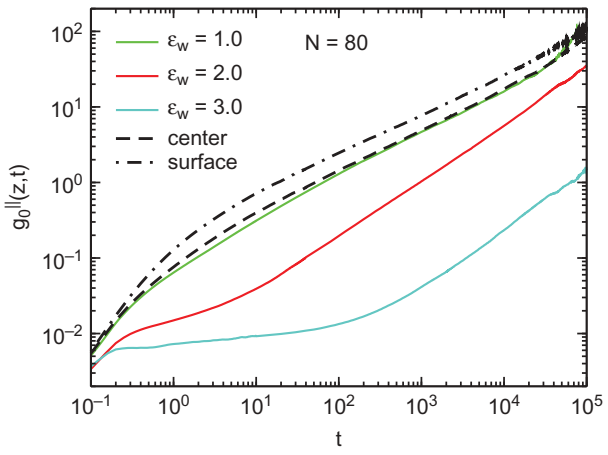

Fig. 16. Lateral mean square displacements (MSD), $g_0^{||}(t)$, for all monomers of polymers with chain length of $N = 80$ inside the adsorption layer ($0.0 < z < 1.4$) as a function of the time t. A plateau gradually develops with increasing ϵ_w as denoted in the legend. In addition, the lateral MSD curves are plotted for the center of the melt and also at the free surface, for comparison. (Here, systems of type C have been studied.) Reproduced from De Virgiliis, et al. (27). © Springer. Reproduced by permission of Springer. Permission to reuse must be obtained from the rightsholder.

indicating that the influence of confining walls on the dynamic properties extends much further than on the conformations of the chains.

The influence of the adsorption strength ϵ_w of the walls on the lateral MSD of those monomers located at the adsorbed layer is considered in Fig. 16, where one can see that by increasing the adsorption strength, a characteristic time interval with low mobility appears. With growing ϵ_w, this interval broadens, indicating that the chain segments predominantly dwell during this time at their original positions. In contrast, when ϵ_w is decreased, the dynamics become faster and for $\epsilon_w = 1.0$ there is almost no differences between interfacial and bulk-like dynamics.

Another way to quantify the structural relaxation across the melt is to consider the incoherent dynamic structure factor:

$$S_q(z,t) = \left\langle \frac{1}{n_t} \sum_i \prod_{t'=0}^{t} \delta(z - z_i(t')) e^{-i\vec{q}\cdot\left[r_i^{||}(t) - r_i^{||}(0)\right]} \right\rangle, \qquad (12)$$

which must also be treated layer-wise (69, 70). In Fig. 17(a) we plotted this function and one can see that an increase in ϵ_w leads to a glassy-like behavior (a typical plateau is developed). One may, therefore, conclude that a process of vitrification of the melt may be initiated by means of increased adhesion to the confining walls whereby the glassy behavior will first apply to the immediate adsorption layer at the attractive wall.

It is thus important to know how vividly an exchange of monomers between the interface and the inner regions of the melt takes place. To this end one may analyze the desorption correlation function, recently introduced by Yelash et al. (13):

$$\phi(t) = \frac{\langle s(t)s(0)\rangle - \langle s\rangle^2}{1 - \langle s\rangle^2}, \qquad (13)$$

where $s(t) = 1$, if at time t the monomer lies at the first adsorbed layer and $s(t) = 0$ otherwise. From Fig.17(b) one may verify that the increase of adhesion rapidly slows down this exchange as ϵ_w is gradually increased.

Two characteristic times τ_s and τ_ϕ can be extracted from Figs. 17(a) and (b), respectively. To this end, we employed a fit of the data to a stretched exponential decay. In Fig. 18(a), τ_s and τ_ϕ are plotted against the adsorption strength ϵ_w. In Fig. 18(b), τ_s and τ_ϕ are plotted against $\langle\rho_s\rangle$, which is the average surface density of monomers at the interface, obtained from the area under the first peak in the monomer number density profile, $\rho(z)$. It should be noted that the relaxation in direction parallel to the substrate determines $S(q_0,t)$, whereas function $\phi(t)$ that appears in Fig. 17(b) reflects mainly the monomer dynamics in the perpendicular direction to the substrate.

Obviously, both characteristic times, τ_s and τ_ϕ, increase nearly exponentially over four orders of magnitude with increasing the adhesion to the substrate ϵ_w, which is similar to

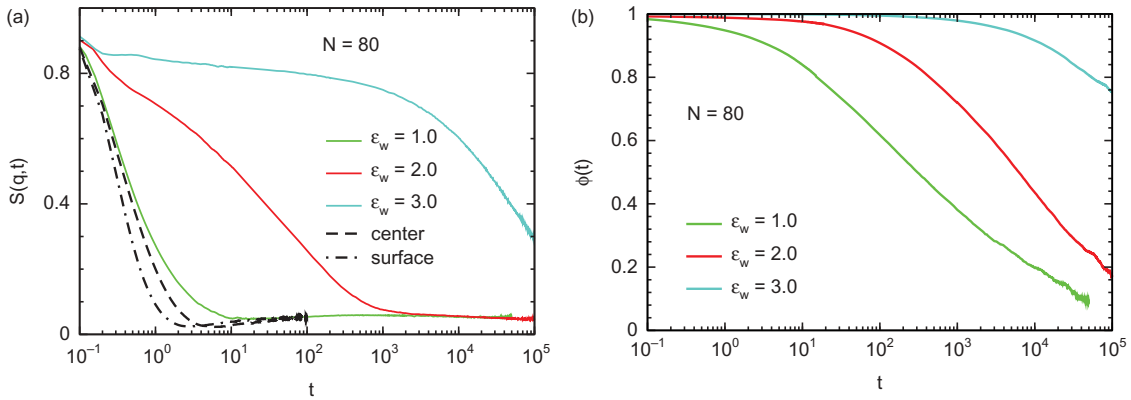

Fig. 17. (a) Plot of the incoherent scattering function, $S(q_0,t)$, for the parallel displacements of monomers with respect to the wall in the adsorption layer for polymers with chain length of $N = 80$, and for three different values of ϵ_w as indicated in the legend, as a function of time t. The same quantity at the center of the bulk and at the free surface are also plotted for comparison. (b) The desorption correlation function for monomers, $\phi(t)$, as a function of time t for various values of the adsorption potential strength $\epsilon_w = 1.0$, 2.0, and 3.0. (Here, systems of type C have been studied.)

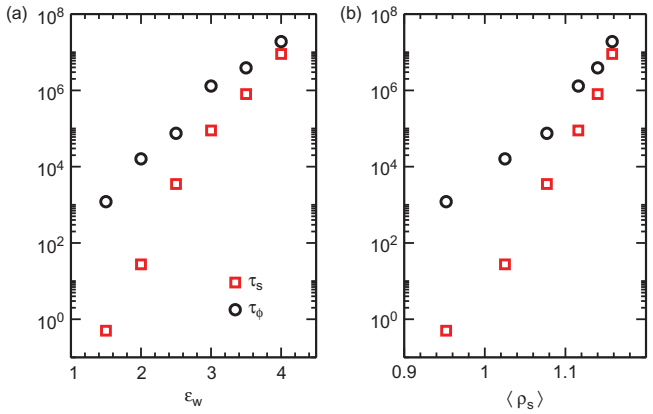

Fig. 18. (a) Plot of the relaxation times, τ_s and τ_ϕ, for monomers at the adsorbed layer, as obtained from $S(q,t)$ (squares) and from $\phi(t)$ (circles), respectively, against the adsorption potential strength ϵ_w. (b) The same as (a) but here the data are plotted against $\langle \rho_s \rangle$, which is the average surface density of monomers at the interface, obtained from the area of the first peak in the monomer number density profile, $\rho(z)$. (Here, systems of type C have been studied.) Reproduced from De Virgiliis, et al. (27). © Springer. Reproduced by permission of Springer. Permission to reuse must be obtained from the rightsholder.

the increase of the viscosity upon vitrification. By growing surface monomer density a similar trend is observed, cf. Fig. 18(b). Such behavior is in good agreement with previous "free volume" theories of the glass transition (71).

Effects of Surface Roughness on the Mobility of Monomers in the Melt

Finally, in this section, we consider the polymer dynamics near the attractive rough solid surface. In order to study the influence of the different levels of the roughness on the dynamics of the melt at interfaces, we investigate systems with different pillar grafting densities as explained in the previous sections. Herein, the interactions between monomers and pillar particles are described by attractive LJ forces with a cut-off radius of 2.5 and a potential well depth of $\epsilon_{\text{phil}} = 2$ (as of the flat wall). In this way the pillars cannot be distinguished energetically from the attractive wall by the polymer melt, and thus it is only the topological effect that affects the polymer dynamics.

In order to compare the dynamics of the system in the bulk to that in the vicinity of the attractive surface, for various values of pillars grafting density, ρ_r, we used type B systems where the the top repulsive surface is located at a distance of $z = 50$ from bottom attractive wall, to create a free surface of the melt under that upper repulsive wall. Therefore, the polymer melt is always at zero normal pressure for different values of ρ_r.

As we mentioned in the Dynamic Properties, Flat Wall section, the polymer melt dynamics is thus anisotropic due to the presence of two interfaces and must be analyzed layerwise. Thus, in this section, we divide the system into layers (slabs) and consider the mobility of the polymers in four qualitatively different slabs. The slabs have thickness of 5σ except for the layer in the bulk, which has the thickness of 10σ, and they are chosen parallel to the walls.

To calculate the lateral MSD, we use $g_0^{||}(z,t)$, which has been defined in Eq. (10), whereby we have taken into account only those n_t monomers that remain in the first ($0 < z < 5$), second ($5 < z < 10$), and third ($10 < z < 15$) layers, and also in the bulk of the system at all times $t' \leq t$. Here, we assume that the distance between the center of mass of each layer from the bottom attractive wall is z.

In Figs. 19 wepresent the normalized diffusion coefficient of the system, which is normalized by the values in the bulk, for the dynamics parallel to the attractive rough wall. The dimensionless quantity $D_{||}/D_{||\text{bulk}}$ is considered as a function of the normalized distance between nearest neighboring pillars, $X/\sqrt{\langle R_g^2 \rangle}$, where $\sqrt{\langle R_g^2 \rangle}$ is the the mean value of the gyration radius in the bulk.

Evidently, the mobility of the monomers in the first layer near the attractive wall is significantly reduced by approximately two orders of magnitude. $D||/D_{||\text{bulk}}$ decreases dramatically whenever $X/\sqrt{\langle R_g^2 \rangle} \leq 2$. Below this threshold, the diminishing distance between the neighboring pillars creates bottlenecks for the polymer coils. As the polymer melt is composed of comparatively short polymers with no mutual entanglements, the strong decrease in lateral diffusion coefficient suggests that the polymer coils at $X/\sqrt{\langle R_g^2 \rangle} \leq 2$ are trapped between neighboring pillars. The latter form effective traps (cavities) such that escape from the trap may occur only by means of other types of dynamics, namely, by reptational motion. As the pillars in this case attract the polymers as strongly as the solid wall, the traps are purely entropic in nature and form a kind of static cavity in the melt that captures those polymers that fit in size for a longer period of time.

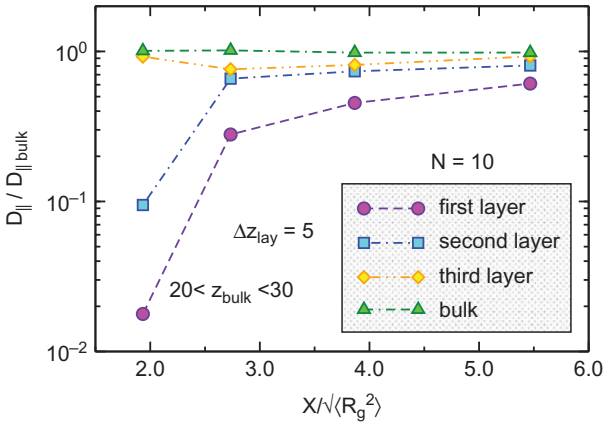

Fig. 19. Normalized lateral diffusion coefficient of the system as function of the distance X between neighboring pillars, normalized by the average value of the gyration radius of a chain in the bulk of the system, $\sqrt{\langle R_g^2 \rangle}$. Here, data are shown from different regions of the first, second and the third layer as well as from the bulk of the system. Chain length is $N = 10$. (Here, systems of type B have been studied.) Reproduced from Sarabadani, J., et al. (45). ©2014, AIP Publishing LLC. Reproduced by permission of AIP Publishing LLC. Permission to reuse must be obtained from the rightsholder.

For the second layer (slab II) a similar observation was also determined. One can see that the reduction in the lateral diffusion coefficient is not so strongly pronounced as in slab I. In the third layer, which corresponds to the slab immediately *above* the pillars, lateral diffusion becomes almost the same as in the bulk as the chains in this layer have only few segments that partially reside in the lower slab and slow down diffusion.

Based on the aforementioned findings one may conclude, therefore, that the roughness of the wall can dramatically slow down the polymer dynamics whenever the polymer's size in the melt becomes comparable or smaller than the characteristic scale of surface roughness.

Conclusion

The structural and dynamic properties of a polymer melt comprised of linear macromolecules in contact with solid walls have been studied for polymer chains of different size N under the influence of different degrees of adhesion and roughness by means of MD simulations of a coarse-grained bead-spring model of homopolymers. Thereby, a number of interesting observations have been made from which several important conclusions can be drawn.

- We have found that the adsorbed amount of monomers, Γ, follows a simple relation $\Gamma(N) \sim N^{1/2}$ for various values of the attractive wall potential, ϵ_w, which is in full agreement with previous theoretical results (50). Moreover, we demonstrated that on the average the length of loops and trains does not depend significantly on ϵ_w whereas by increasing of ϵ_w the number of loops and trains as a whole slightly decreases. In addition, on the average the length of the tails grows linearly with the polymer size, N, for a fixed value of the strength ϵ_w which confirms the theoretical studies of Scheujtens and Fleer (32).
- Quite interestingly, our considerations revealed that the conformational properties of the chains in a melt, which is in contact with hard solid wall, resemble closely those of a single polymer chain at a surface under critical adsorption conditions, regardless of the particular interaction between hard wall and chains, in agreement with the Silberberg's hypothesis. Minor deviations, observed immediately at the walls, are due to surface layering effects, yet they do not distort the overall picture of ideal chains under reflective boundary conditions.
- Our studies also showed that the pressure of the confined melt, $P_N - P_\infty$, decreases with increasing chain length N as $1/N$, which we interpret as an effect of the chain-ends. By using the anisotropy of the pressure tensor parallel and perpendicular to the solid surfaces, one can obtain the surface tension of the melt, which is here found to decay at solid substrates as $\gamma_N - \gamma_\infty \propto N^{-2/3}$, in good agreement with earlier experimental observations.
- In order to test the dynamical behavior of the polymer melt under confinement, we have also considered z-dependent mean square displacements of monomers, Eq. (10), in both parallel and perpendicular directions to the solid substrate. This investigations indicate that monomer mobility is influenced by the particular type of interface (solid wall or free surface), whereby surface adhesion induces typical glassy dynamics in the layer adjacent to the attractive wall. Eventually, we determined that the mobility of polymers near attractive rough surfaces dramatically decreases when the typical scale of the surface roughness becomes comparable to the mean coil size in the bulk of the system. In this case, we refer the observed drop in polymer mobility to the crossover from Rouse- to the much slower reptation dynamics (54) that the polymers have to undergo in order to escape from the entropic traps imposed by the wall roughness.

Acknowledgements

We are indebted to A. M. Skvortsov for stimulating discussions on the problem and V. Rostiashvili for careful reading of the manuscript. J. S. thanks K. Kremer, B. Dünweg, D. Mukherji, K. Daoulas, D. Andrienko, F. Varnik, and S. Neogi for enlightening discussions. J. S. is grateful to T. Stuehn, V. Starchenko, and K. Koschke for their helps on using ESPResSo++ package.

Funding

The DFG support through the SPP 1369 *Solid-polymer contacts: interfaces and interphases* is hereby gratefully acknowledged.

References

1. Fleer, G. J., Cohen-Stuart, M. A., Scheutens, J. M. H. M., and Cosgrove, T. (1993) *Polymers at Interfaces*; Chapmann-Hall: London.
2. Wu, S. (1982) *Polymer Interface and Adhesion*; Marcel Dekker: New York.
3. Skvortsov, A. M., Leermakers, F. A. M., and Fleer, G. J. (2013) *J. Chem. Phys.*, 139:054907.
4. Varnik, F., and Binder, K. (2009) *Int. J. Mat. Res.*, 100:1494.
5. Daoulas, K. Ch., Harmandaris, V. A., and Mavrantzas, V. G. (2005) *Macromolecules*, 38:5780.
6. Harmandaris, V. A., Daoulas, K. Ch., and Mavrantzas, V. G. (2005) *Macromolecules*, 38:5796.
7. Mansfield, K. F., and Theodorou, D. N. (1989) *Macromolecules*, 22:3143.
8. Mansfield, K. F., and Theodorou, D. N. (1990) *Macromolecules*, 23:4430.
9. Mansfield, K. F., and Theodorou, D. N. (1991) *Macromolecules*, 24:4295.
10. Mansfield, K. F., and Theodorou, D. N. (1991) *Macromolecules*, 24:6293.
11. Smith, G. D., Yoon, D. Y., and Jaffe, R. L. (1992) *Macromolecules*, 25:7011.
12. Pandey, Y. N., and Doxastakis, M. (2012) *J. Chem. Phys.*, 136:094901.
13. Yelash, L., Virnau, P., Binder, K., and Paul, W. (2010) *Phys. Rev. E*, 82:050801R.
14. Hentschke, R., Schurmann, B. L., and Rabe, J. P. (1992) *J. Chem. Phys.*, 96:6213.
15. Pandey, R., Milchev, A., and Binder, K. (1997) *Macromolecules*, 30:1194.
16. Baschnagel, J., Binder, K., and Milchev, A. (2000) *Polymer Surfaces, Interfaces, and Thin Films*; Karim A., and Kumar, S., eds., World Scientific Publ. Co: Singapore, p. 1.
17. Bitsanis, I. A., and ten Brinke, G. (1993) *J. Chem. Phys.*, 99:3100.
18. Cavallo, A., Müller, M., Wittmer, J. P., Johner, A., and Binder, K. (2005) *J. Phys. Condens. Matter*, 17:S1697.
19. Bitsanis, I., and Hadziioannou, G. (1990) *J. Chem. Phys.*, 92:3827.
20. Varnik, F., Baschnagel, J., and Binder, K. (2000) *J. Chem. Phys.*, 113:4444.

21. Peter, S., Meyer, H., and Baschnagel, J. (2006) *J. Polym. Sci. B*, 44:2951.
22. Desai, T. G., Keblinski, P., and Kumar, S. K. (2008) *J. Chem. Phys.*, 128:044903.
23. Smith, G. D., Bedrov, D., and Borodin, O. (2003) *Phys. Rev. Lett.*, 90:226103.
24. Mukherji, D., and Müser, M. H. (2007) *Macromolecules*, 40:1754.
25. Winkler, R. G., Matsuda, T., and Yoon, D. Y. (1993) *J. Chem. Phys.*, 98:729.
26. Matsuda, T., Smith, G. D., Winkler, R. G., and Yoon, D. Y. (1995) *Macromolecules*, 28:165.
27. De Virgiliis, A., Milchev, A., Rostiashvili, V. G., and Vilgis, T. A. (2012) *Europ. Phys. J. E.*, 35:97.
28. Eslami, H., and Müller-Plathe, F. (2013) *J. Phys. Chem. C*, 117:5249.
29. Eslami, H., and Behrouz, M. (2014) *J. Phys. Chem. C*, 118:9841.
30. Eslami, H., Rahimi, M., and Müller-Plathe, F. (2013) *Macromolecules*, 46:8680.
31. Johnston, K., and Harmandaris, V. (2013) *Macromolecules*, 46:5741.
32. Scheujtens, J. M. H. M., and Fleer, G. J. (1980) *J. Phys. Chem.*, 84:178.
33. Fleer, G. J., van Male, J., and Johner, A. (1999) *Macromolecules*, 32:825.
34. Fleer, G. J., van Male, J., and Johner, A. (1999) *Macromolecules*, 32:845.
35. Baschnagel, J., and Varnik, F. (2005) *J. Phys.: Condens. Matter*, 17:R851.
36. Scheidler, P., Kob, W., and Binder, K. (2002) *Europhys. Lett.*, 59:701.
37. Scheidler, P., Kob, W., and Binder, K. (2004) *J. Phys. Chem. B*, 108:6673.
38. Adriani, P. M., and Chakraborty, A. K. (1993) *J. Chem. Phys.*, 98:4263.
39. Peter, S., Napolitano, S., Meyer, H., Wübbenhorst, M., and Baschnagel, J. (2008) *Macromolecules* 41:7729.
40. Kutvonen, A., Rossi, G., and Ala-Nissila, T. (2012) *Phys. Rev. E*, 85:041803.
41. Knauert, S. T., Douglass, J. F., and Starr, F. W. (2010) *Macromolecules*, 43:3438.
42. Silberberg, A. (1988) *J. Colloid Interface Sci.*, 90:86.
43. Silberberg, A. (1988) *J. Colloid Interface Sci.*, 125:14.
44. Skvortsov, A. M., and Gorbunov, A. A. (1986) *Vysokomol. Soed.*, 28:1941–1946.
45. Sarabadani, J., Milchev, A., and Vilgis, T. A. (2014) *J. Chem Phys.*, 141:044907.
46. Hoeve, C. A. J., Di Marzio, E. A., and Peyser, P. (1965) *J. Chem. Phys.*, 42:2558.
47. Grest, G. S., and Kremer, K. (1986) *Phys. Rev. A*, 33:3628.
48. Halverson, J. D., Brandes, T., Lenz, O., Arnold, A., Bevc, S., Starchenko, V., Kremer, K., Stuehn, T., and Reith, D. (2013) *Comp. Phys. Commun.*, 184:1129.
49. Todorov, I. T., Smith, W., Trachenko, K., and Dove, M. T. (2006) *J. Mater. Chem.*, 16:1911.
50. Scheutjens, J. M. H. M., and Fleer, G. J. (1980) *J. Phys. Chem.*, 84:178.
51. Milchev, A., and Binder, K. (2001) *J. Chem. Phys.*, 114:8610.
52. Eisenriegler, E., Kremer, K., and Binder, K. (1982) *J. Chem. Phys.*, 77:6296.
53. Klushin, L. I., Polotsky, A. A., Hsu, H.-P., Markelov, D. A., Binder, K., and Skvortsov, A. M. (2013) *Phys. Rev. E*, 87:022604.
54. Doi, M., and Edwards, S. F. (1986) *The Theory of Polymer Dynamics*; Oxford University Press: New York.
55. ten Brinke, G., Ausserre, D., and Hadziioannou, G. (1988) *J. Chem. Phys.*, 89:4374.
56. Kumar, S. K., Vacatello, M., and Yoon, D. Y. (1988) *J. Chem. Phys.*, 89:5206.
57. Theodorou, D. N. (1988) *Macromolecules*, 21:1391.
58. Theodorou, D. N. (1988) *Macromolecules*, 21:1400.
59. Irving, J. H., and Kirkwood, J. G. (1950) *J.Chem. Phys.*, 18:817.
60. Hansen, J. -P., and McDonald, I. R. (1990) *Theory of Simple Liquids*; Academic: London.
61. Pathria, R. K. (2001) *Statistical Mechanics*; Butterworth Heinemann.
62. Rowlinson, J. S., and Widom, B. (1982) *Molecular Theory of Capillarity*; Clarendon: Oxford.
63. Milchev, A., and Binder, K. (2001) *J. Chem. Phys.*, 114:8610.
64. Cahn, J. W., and Hilliard, J. E. (1958) *J. Chem. Phys.*, 28:258.
65. Poser, C. I., and Sanchez, I. C. (1979) *J. Colloid Interface. Sci.*, 69:539.
66. Legrand, D. G., and Gaines, G. L. (1969) *J. Colloid Interface Sci.*, 31:162.
67. Sauer, B. B., and Dee, G. T. (1994) *Macromolecules*, 27:6112–6116.
68. Wu, S. (1974) *J. Macromol. Sci. - Revs. Macromol. Chem.*, C10:1–73.
69. Peter, S., Meyer, H., Baschnagel, J., and Seemann, R. (2007) *J. Phys.: Condens. Matter*, 19:205119.
70. Smith, G.D., Bedrov, D., and Borodin, O. (2003) *Phys. Rev. Lett.*, 90:226103.
71. Adam, G., and Gibbs, J. H. (1965) *J. Chern. Phys.*, 43:139.